

Article

Recent Advances Concerning the ^{87}Sr Optical Lattice Clock at the National Time Service Center

Yebing Wang ^{1,2} , Xiaotong Lu ^{1,2}, Benquan Lu ¹, Dehuan Kong ^{1,2} and Hong Chang ^{1,*}

¹ Key Laboratory of Time and Frequency Primary Standards, National Time Service Center, Chinese Academy of Sciences, Xi'an 710600, China; wangyebing@ntsc.ac.cn (Y.W.); 13980960458@163.com (X.L.); lubenquan@126.com (B.L.); kongdehuan@ntsc.ac.cn (D.K.)

² School of Astronomy and Space Science, University of Chinese Academy of Sciences, Beijing 100049, China

* Correspondence: changhong@ntsc.ac.cn; Tel.: +86-029-8389-0852

Received: 27 September 2018; Accepted: 5 November 2018; Published: 8 November 2018



Abstract: We review recent experimental progress concerning the ^{87}Sr optical lattice clock at the National Time Service Center in China. Hertz-level spectroscopy of the ^{87}Sr clock transition for the optical lattice clock was performed, and closed-loop operation of the optical lattice clock was realized. A fractional frequency instability of 2.8×10^{-17} was attained for an averaging time of 2000 s. The Allan deviation is found to be $1.6 \times 10^{-15} / \tau^{1/2}$ and is limited mainly by white-frequency-noise. The Landé g -factors of the $(5s^2)^1S_0$ and $(5s5p)^3P_0$ states in ^{87}Sr were measured experimentally; they are important for evaluating the clock's Zeeman shifts. We also present recent work on the miniaturization of the strontium optical lattice clock for space applications.

Keywords: optical clocks; strontium atoms; optical lattices; laser cooling and trapping; stability; uncertainty

1. Introduction

Because of their potential to provide high Q factors than those of microwave clocks, optical atomic clocks offer a tremendous advantage in both short-term and long-term stability in comparison with conventional microwave clocks [1,2]. In the last few decades, optical clocks employing neutral atoms [3–6] and single ions [7–9] have progressed remarkable regarding instability and achieving uncertainty levels of 10^{-18} , surpassing the cesium primary frequency standard as the definition for the second of the International System of Units. The great progress in optical clocks over the past decade has immensely influenced developments in science and technology areas such as topological dark matter hunting [10], gravitational wave detection [11], fundamental physics measurement [12–14], quantum simulators and geodetic applications [15–17].

Alkaline earth(-like) atoms are the most promising candidates for optical lattice clock among possible atomic candidates because of their abundant and special energy levels. A large number of strontium optical lattice clocks [18] are currently under development world-wide with uncertainties of up to a few parts in 1×10^{-18} [3,5,6]. Recently, the team at the Joint Institute for Laboratory Astrophysics (JILA) obtained using an ^{87}Sr optical lattice clock [19] a measurement precision of 5×10^{-19} in 1 h of averaging time by taking advantage of the high, correlated density of a degenerate Fermi gas in a three-dimensional optical lattice to guard against on-site interaction shifts.

In this article, we report recent experimental progress concerning our ^{87}Sr optical lattice clock at the National Time Service Center. The organization of this paper is as follows. First, recent progress with the clock is described. Second, the experimental determination of the Landé g -factors for $(5s^2)^1S_0$ and $(5s5p)^3P_0$ states of ^{87}Sr is presented. Finally, we mention work on the miniaturization of strontium optical lattice clock for future space applications.

2. Optical Lattice Clock Based on ^{87}Sr

2.1. Level Structure and Cooling Transitions of ^{87}Sr

The relevant energy levels of ^{87}Sr with transitions and wavelengths used in an optical lattice clock are shown in Figure 1.

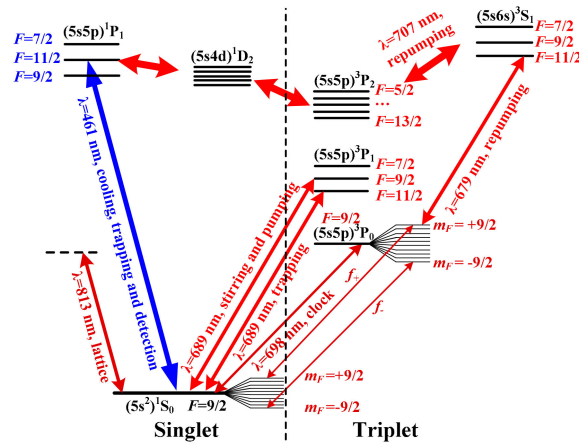


Figure 1. Energy level scheme of the ^{87}Sr atom.

An oven, which is heated to a temperature of $500\text{ }^{\circ}\text{C}$, emits a strontium atomic beam at a velocity of 460 m/s . A Zeeman slower formed with ten coils and 461-nm laser is used to slow the velocity of the thermal atomic beam to about 50 m/s . The strontium atoms are further cooled and trapped in a two-stage magneto-optical trap (MOT). The strong dipole-allowed $(5s^2)^1S_0(F = 9/2) - (5s5p)^1P_1(F = 11/2)$ transition (461-nm , 32-MHz natural linewidth) is used for the first Doppler cooling stage; the corresponding cooling limit is roughly in the sub-millikelvin range. With the 679-nm and 707-nm lasers, optical repumping returns the $(5s5p)^3P_2$ and $(5s5p)^3P_0$ metastable states to the ground state $(5s^2)^1S_0$ to cool and trap more atoms. The intercombination $(5s^2)^1S_0(F = 9/2) - (5s5p)^3P_1(F = 11/2)$ transition (689-nm , 7.5-kHz natural linewidth) between the singlet and triplet states is used in the second Doppler cooling stage; the corresponding cooling limit is near the sub-microkelvin range. A stirring laser corresponding to the $(5s^2)^1S_0(F = 9/2) - (5s5p)^3P_1(F = 9/2)$ transition provides a rapid randomization among the ten Zeeman sublevels of the $(5s^2)^1S_0$ state. Additionally, it is also used as a pump laser to drive the entire population of the ten Zeeman sublevels to the $m_F = +9/2 - m_F = +9/2$ and $m_F = -9/2 - m_F = -9/2$ sublevels.

After this two-stage cooling and trapping, roughly 3.5×10^6 atoms are trapped in the red MOT with a temperature of $3.9\text{ }\mu\text{K}$. The one-dimensional (1-D) horizontally oriented optical lattice is operated at 813 nm and traps the cooled atoms in the Lamb-Dicke regime [20]. The $(5s^2)^1S_0 - (5s5p)^3P_0$ transition at 698 nm is used as the clock line because of its narrow natural linewidth of about 1 mHz .

2.2. Fiber Phase Noise Cancellation

The 698-nm grating-stabilized diode laser is stabilized to an ultra-low-expansion (ULE) cavity, having a finesse of about 4×10^5 with the Pound-Drever-Hall (PDH) technique. The length and orientation of the ULE cavity at 698 nm placed in vacuum are 10 cm and horizontal, respectively. The linewidth of the clock laser is about 1 Hz and the power is 5 mW . The clock laser beam is sent to the cold atoms for probing using a 5-m-long polarization-maintaining optical fiber with a transmission efficiency of about 80% . The fiber introduces a lot of phase noise, which translates into frequency noise and eventually a loss of spectral purity. To maintain the optical coherence of the clock laser source with the strontium cold atoms, we applied an efficient fiber-noise-cancellation (FNC) system. We introduce noise compensation directly at the input of the fiber with an acousto-optic modulator (AOM), where a part of the light comes from the reflected light that is inputted and reflected back from the output end of the fiber; the rest part of the light is used as a reference. It is possible to obtain a

beat signal introduced by the fiber phase noise from the beat signal of the two parts but has a high frequency [21–23].

The error signal at low frequency can be obtained directly by mixing the beat signal with a local reference oscillator. The error signal is then used to modulate a voltage-controlled-oscillator (VCO) that drives the AOM around 80 MHz.

Figure 2a shows the frequency fluctuation of the beat signal with and without the FNC system. With the FNC active, the frequency fluctuation caused by the residual phase noise is reduced below 40 MHz and is sufficiently low for transferring a 1-Hz linewidth laser beam. Figure 2b shows the optical field spectral density of the beat signal with and without FNC, measured with a spectrum analyzer. Figure 2c shows the frequency instability caused by fiber noise when the FNC system is active, obtained by measuring directly the Allan deviation for our phase-locked system. Affected by white phase noise, the Allan deviation of the phase noise cancellation system follows a τ^{-1} behavior.

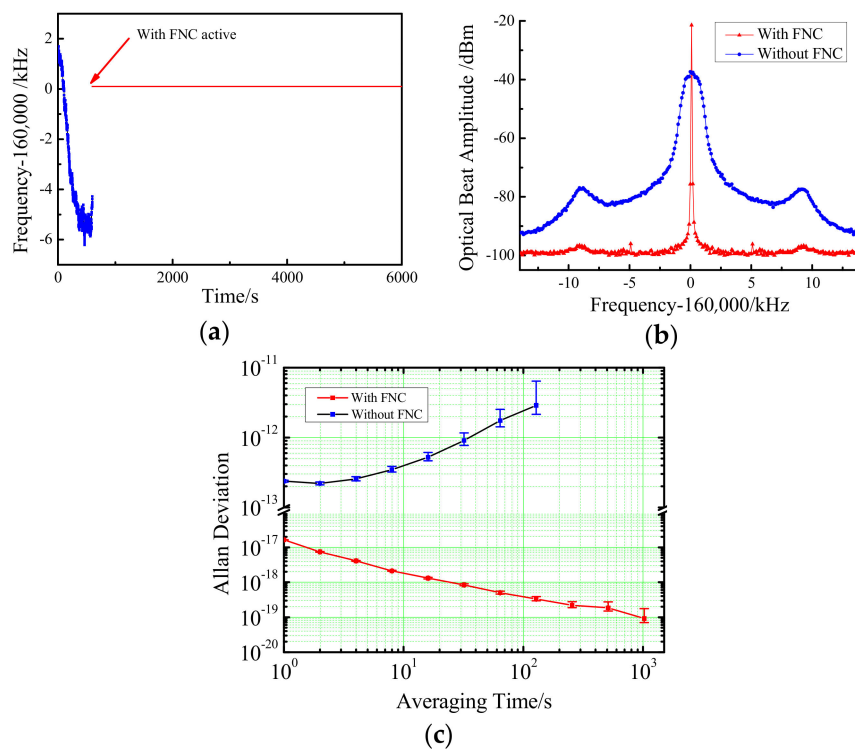


Figure 2. (a) Frequency fluctuation of the beat signal with and without the FNC system; (b) Optical field spectrum of the beat signal with and without the FNC system; (c) In loop frequency stability (Allan deviation) of the FNC system. The data sample has a 1-s gate time.

2.3. Lifetime of Atoms in the Lattice

A laser operating at wavelength 813 nm is used to configure a 1-D horizontally oriented optical lattice. The 813-nm ECDL is stabilized to an ULE optical reference cavity, having a finesse of about 3×10^4 , using the PDH technique. The 813-nm lattice laser beam was focused to a waist size of 120 μm ; the depth of the trap lattice is about 56 E_r , where E_r is the lattice photon recoil energy. About 10^4 atoms are then loaded into the 1-D optical lattice at a magic wavelength of 813.4 nm.

An image of the 1-D optical lattice with a falling time of 30 ms is shown in Figure 3a. The line above is an in-situ image of the atoms trapped in the lattice; the cloud below is the atomic distribution after time-of-flight imaging. From fitting an exponential decay function (Figure 3b), the $1/e$ lifetime of the 1-D lattice is about 1.6 s. A long lattice lifetime is useful in resolving the narrow spectroscopy of the clock transition.

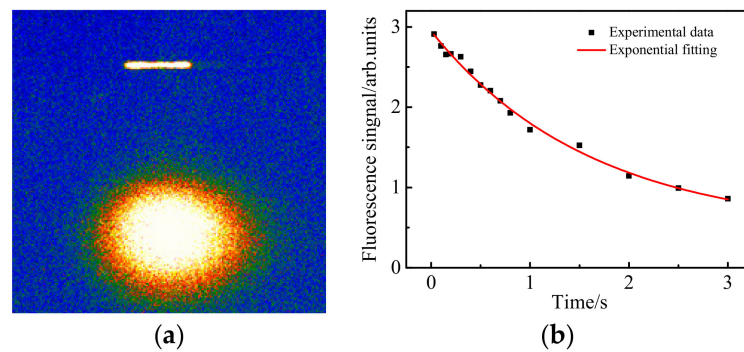


Figure 3. (a) Image of the 1-D optical lattice; (b) Lifetime of the atoms trapped in the optical lattice.

2.4. Clock Transition Spectra of ^{87}Sr

Using the normalized shelving method [5,6], resolved sideband spectroscopy of the ^{87}Sr clock transition was performed (Figure 4a). The clock transition spectroscopy indicates that the atomic longitudinal temperature is about $4.2\ \mu\text{K}$. With decreasing power and frequency range of the clock laser, a high-resolution spectrum of the clock transition (Figure 4b) was obtained when the atoms–laser interaction time was 150 ms and shows a linewidth of 6.7 Hz.

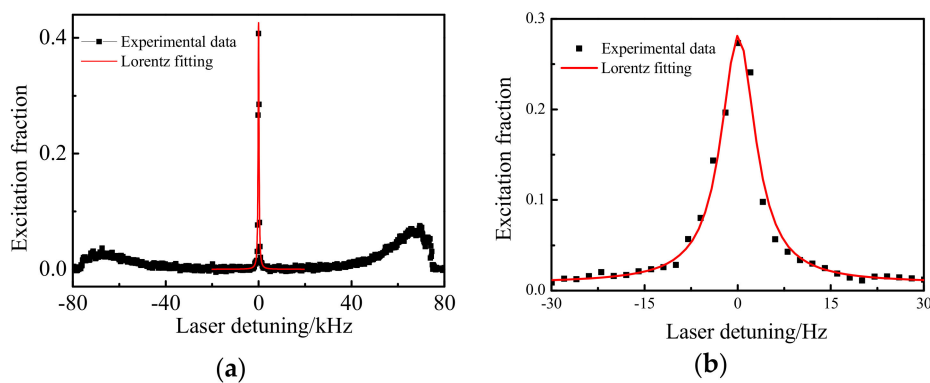


Figure 4. (a) Resolved sideband spectrum of the ^{87}Sr clock transition; (b) High resolution carrier spectrum of the clock transition.

With a small bias magnetic field of 0.3 G applied along the polarization axis of the lattice light, spectra of the π transitions were observed and ten Zeeman peaks were separated (Figure 5a). The intensity of individual π -polarized transitions depends on values of the Clebsch-Gordan coefficients. To avoid wasting the atomic population, atoms in all the m_F states were prepared in the $(5s^2)^1S_0(m_F = +9/2)$ or $(5s^2)^1S_0(m_F = -9/2)$ stretched states via the 689-nm σ^+ or σ^- polarized laser resonance excitation. The pumping laser beam propagates along the polarization axis of clock and lattice lasers and its polarization is switched between σ^+ and σ^- polarization using a liquid crystal variable wave plate. As a result, about 90% of the population were driven into the two sublevels; the population of the excited clock states is about seven times higher than that without the pumping laser beam. Finally, the linewidth of the two magnetic sublevels transition are 6.8 Hz and 6.2 Hz respectively (Figure 5b). The narrowest linewidth of the magnetic sublevel transitions that we can obtain at present is 4.9 Hz with a probing time of 300 ms (Figure 5c).

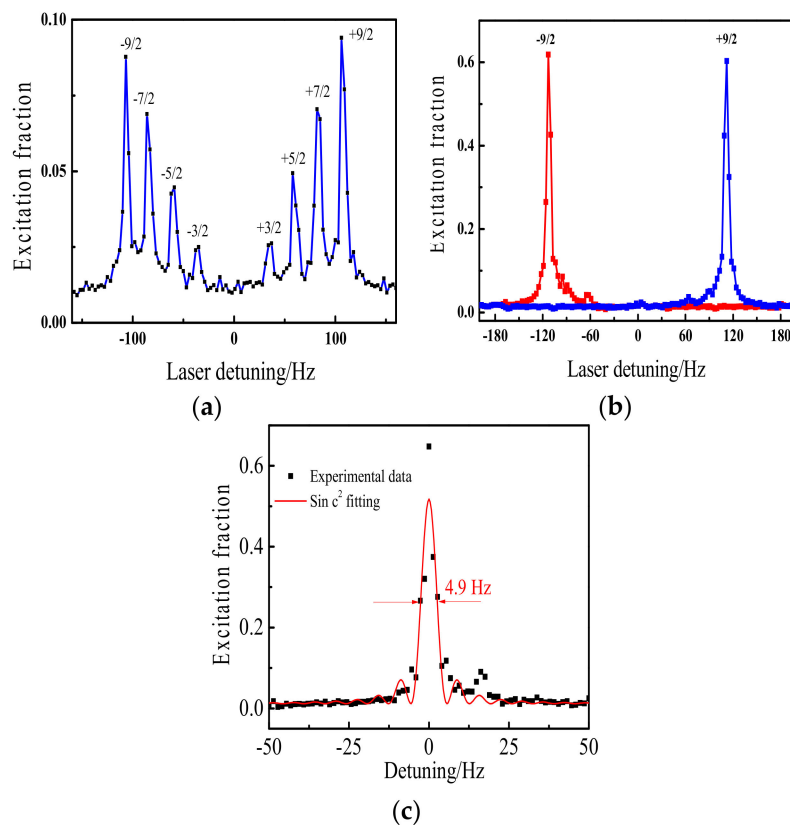


Figure 5. (a) Spectra of the π transitions in the presence of a 0.3-G magnetic field; (b) Spin-polarized spectra for the transitions $m_F = +9/2$ - $m_F = +9/2$ and $m_F = -9/2$ - $m_F = -9/2$; (c) Narrowest linewidth of the magnetic sublevel transitions.

2.5. Closed-Loop Operation of ^{87}Sr Optical Lattice Clock

In the experimental setup for our ^{87}Sr optical lattice clock (Figure 6), a clock laser operating at 698-nm, locked to an ULE cavity using the PDH technique, delivers a beam to a cold atom sample. The clock transition is detected using the electron-shelving technique for the transition $(5s^2)^1S_0$ - $(5s5p)^1P_1$. A normalization scheme is used to eliminate the shot-to-shot noise [24]. To stabilize the clock laser to resonate at the atomic transition of $(5s^2)^1S_0$ - $(5s5p)^3P_0$, we applied the modulation method. We stabilized the clock laser to the average frequency of the two $m_F = +9/2$ - $m_F = +9/2$ and $m_F = -9/2$ - $m_F = -9/2$ Zeeman transitions. The error signal is calculated digitally from four clock cycle. After filtering using a PID (proportional, integral, derivative) controller, feedback is provided by a frequency correction signal to modulate the AOM2 [25].

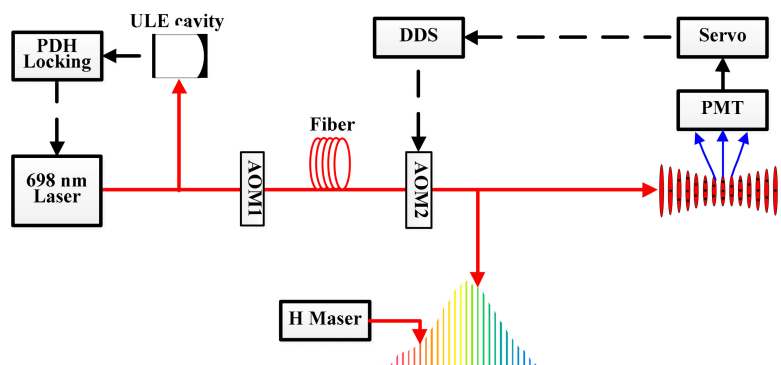


Figure 6. Schematic diagram of the experimental setup for ^{87}Sr optical lattice clock. (DDS: direct digital synthesizer; PMT: photomultiplier tube; PDH: Pound-Drever-Hall).

The error signal was obtained after the clock laser had been locked to the atomic transition (Figure 7a) along with the in-loop error signal stability of the ^{87}Sr optical lattice clock (Figure 7b). Short-term stability is limited by the clock laser and is affected by the length fluctuation of the ULE cavity; long-term stability is also limited by the clock transition of ^{87}Sr . The fractional frequency instability obtained was 2.8×10^{-17} for an averaging time of 2000 s. The Allan deviation is fitted with $1.6 \times 10^{-15}/\tau^{1/2}$, which is limited mainly by white-frequency-noise.

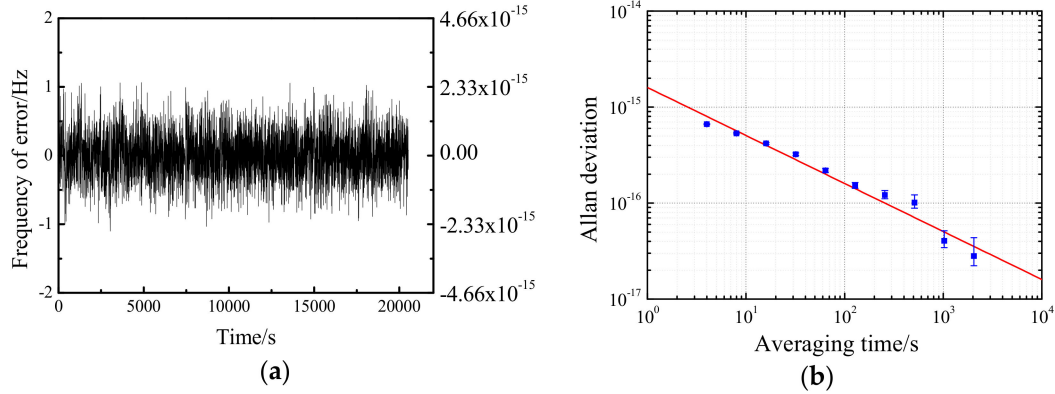


Figure 7. (a) Error signal after the clock laser locked to the atomic transition; (b) In-loop fractional frequency instability of the ^{87}Sr optical lattice clock.

3. Experimental Determination of the Landé g -Factors for $(5s^2)^1S_0$ and $(5s5p)^3P_0$ States of ^{87}Sr

Because the clock transition frequency is sensitive to both first- and second-order Zeeman shifts, the value of the Landé g -factors of the clock states need to be determined accurately [26]. We measured experimentally the g -factors of the ground state $(5s^2)^1S_0$ and the differential g -factor δg between the $(5s5p)^3P_0$ and $(5s^2)^1S_0$ states of ^{87}Sr with π -polarized and σ^\pm -polarized interrogation beams, respectively, at different magnetic field strengths [27]. A typical spectrum of the π -transition is shown in Figure 5a. When the polarization direction of the clock laser is perpendicular to the direction of the magnetic field, the σ^\pm -transition spectrum is obtained (Figure 8a). These peaks correspond to the transitions between the ground and excited sublevels. From the σ^\pm -transition spectrum, δg can be expressed as

$$\delta g = \frac{g(5s^2^1S_0)}{\frac{f_{d,mF}}{2f_{\sigma^\pm,mF}} - 1} = \frac{(1 - \sigma_d) g_I}{\frac{f_{d,mF}}{2f_{\sigma^\pm,mF}} - 1}, \quad (1)$$

where the diamagnetic correction $\sigma_d = 0.00345$ [26], $f_{\sigma^\pm,mF}$ is the frequency gap between neighboring lines for the σ^\pm transitions, $f_{d,mF}$ is the frequency difference between σ^+ and σ^- transition from the same sublevel, $g_I = \mu_I/I\mu_0$ with μ_0 the vacuum permeability, and the nuclear magnetic moment $\mu_I = -1.0924(7) \mu_N$ [28] with μ_N the nuclear magneton. By accurately measuring the frequency interval between the two neighboring peaks, the Landé g -factor $g((5s^2)^1S_0)$ (Figure 8b) and the differential g -factor δg (Figure 8c) may be obtained. The values of $g((5s^2)^1S_0)$ and δg may be determined without the calibration of the external magnetic field from the σ^\pm -transition spectra. A final value of $\delta g = -7.72(43) \times 10^{-5}$ is obtained that agrees very well with a previous report [26].

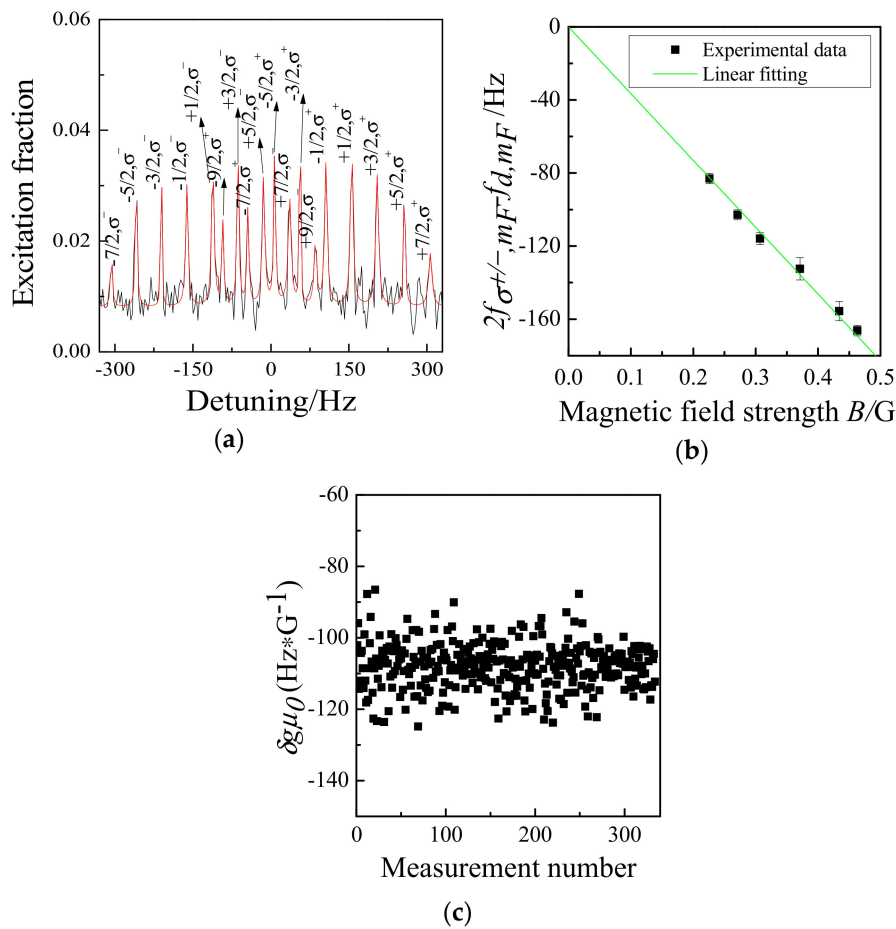


Figure 8. (a) σ^{\pm} -transition spectrum; (b) Measured values of $2f_{\sigma^{\pm}, mF} - f_{d, mF}$ as a function of the magnetic field strength; (c) Measured values of $\delta g\mu_0$ ($\text{Hz}\cdot\text{G}^{-1}$) obtained from the σ^{\pm} -transition spectra.

4. Miniaturization of Strontium Optical Lattice Clock for a Space Optical Clock

Because space is a microgravity environment, an optical clock should achieve higher stability and accuracy than on Earth [29,30]. An optical clock in space may be used in tests of fundamental physics, such as Einstein’s theory of relativity, positioning, time and frequency transfers, accurate geoid determination, and monitoring and deep space navigation.

Making optical clocks compact and robust for transport is the first step towards applications of optical clocks in space [31–33]. We have produced a compact, robust laser source system operating at 461 nm along with a vacuum setup system (Figure 9). With these two systems, the first stage cooling and trapping of the ^{87}Sr atoms have been accomplished [34]. The ECDL 461-nm laser is locked to the $(5s^2)^1S_0 - (5s5p)^1P_1$ transition line of ^{88}Sr . After lock, the residual power of the 461-nm laser is 35 mW. More power is obtained from two other injection-locked slave lasers. The vacuum system includes an atomic oven, a two-dimensional collimating cavity, a Zeeman slower and a MOT cavity. We designed and constructed the Zeeman slower with permanent magnets [34]. With a MOT coil current of 2 A, an axial magnetic field gradient of 43 Gs/cm was obtained in the center of the MOT cavity and satisfies the requirements for the first-stage Doppler cooling very well.

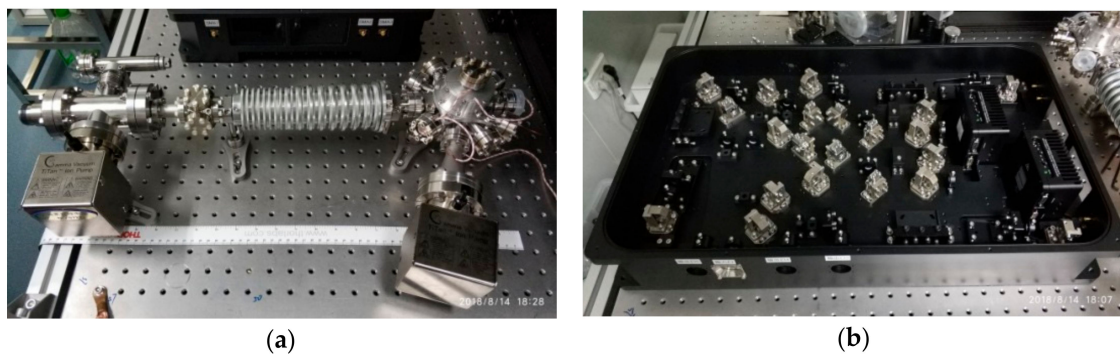


Figure 9. (a) Compact vacuum system of the ^{87}Sr optical lattice clock; (b) Modular 461-nm laser system.

The internal diameter is 1.5 mm and the final temperature of the blue MOT is approximately 10.6 mK, which was determined by observing the expansion of the atoms in this MOT. The number of cold atoms finally trapped in the blue MOT is 1.6×10^6 for ^{88}Sr and 1.5×10^5 for ^{87}Sr . With two repumping lasers operating at 679 nm and 707 nm, the typical number of loaded atoms increased typically five-fold compared with before.

5. Conclusions

We achieved the clock laser stabilization to the atomic transition in an optical atomic clock over a continuous operation of over 8 h. A Hertz-level spectrum of the ^{87}Sr clock transition was obtained. A fractional frequency instability of 2.8×10^{-17} was attained with an averaging time of 2000 s. We plan to evaluate the systematic uncertainty of ^{87}Sr optical lattice clock and measure the absolute frequency of the clock transition using an optical comb that locks to a H-maser. The Landé g -factors of the $(5s^2)^1S_0$ and $(5s5p)^3P_0$ states and the differential g -factor δg between the two states of the ^{87}Sr atom were measured accurately in experiments and are in good agreement with those of a previous report. We have achieved a compact and robust laser source system operating at 461 nm and a vacuum system. To date, the first-stage cooling and trapping of ^{87}Sr atoms have been accomplished.

Author Contributions: Y.W. wrote the manuscript. Y.W. and X.L. performed the experiment. B.L. and D.K. performed the theory. H.C. supervised the study.

Funding: This research was supported by the National Natural Science Foundation of China (Grant Nos. 11474282 and 61775220), the National Key R&D Program of China (Grant No. 2016YFF0200201), the Key Research Project of Frontier Science of the Chinese Academy of Sciences (Grant No. QYZDB-SSW-JSC004) and the Strategic Priority Research Program of the Chinese Academy of Sciences (Grant No. XDB21030100).

Acknowledgments: We would like to thank Longsheng Ma, Baolong Lyu, Lingxiang He and Yige Lin for their helpful discussions.

Conflicts of Interest: The authors declare no conflict of interest. The funders had no role in the design of the study; in the collection, analyses, or interpretation of data; in the writing of the manuscript, and in the decision to publish the results.

References

1. Derevianko, A.; Katori, H. Colloquium: Physics of optical lattice clocks. *Rev. Mod. Phys.* **2011**, *83*, 331–347. [[CrossRef](#)]
2. Ludlow, A.D.; Boyd, M.M.; Ye, J.; Peik, E.; Schmidt, P.O. Optical atomic clocks. *Rev. Mod. Phys.* **2015**, *87*, 637–701. [[CrossRef](#)]
3. Bloom, B.J.; Nicholson, T.L.; Williams, J.R.; Campbell, S.L.; Bishof, M.; Zhang, X.; Zhang, W.; Bromley, S.L.; Ye, J. An optical lattice clock with accuracy and stability at the 10^{-18} level. *Nature* **2014**, *506*, 71–75. [[CrossRef](#)] [[PubMed](#)]
4. Hinkley, N.; Sherman, J.A.; Phillips, N.B.; Schioppa, M.; Lemke, N.D.; Beloy, K.; Pizzocaro, M.; Oates, C.W.; Ludlow, A.D. An atomic clock with 10^{-18} instability. *Science* **2013**, *341*, 1215–1218. [[CrossRef](#)] [[PubMed](#)]

5. Nicholson, T.L.; Campbell, S.L.; Hutson, R.B.; Marti, G.E.; Bloom, B.J.; McNally, R.L.; Zhang, W.; Barrett, M.D.; Safronova, M.S.; Strouse, G.F.; et al. Systematic evaluation of an atomic clock at 2×10^{-18} total uncertainty. *Nat. Commun.* **2015**, *6*, 6896. [[CrossRef](#)] [[PubMed](#)]
6. Ushijima, I.; Takamoto, M.; Das, M.; Ohkubo, T.; Katori, H. Cryogenic optical lattice clocks. *Nat. Photon.* **2015**, *9*, 185–189. [[CrossRef](#)]
7. Chou, C.W.; Hume, D.B.; Rosenband, T.; Wineland, D.J. Optical clocks and relativity. *Science* **2010**, *329*, 1630–1633. [[CrossRef](#)] [[PubMed](#)]
8. Huntemann, N.; Sanner, C.; Lipphardt, B.; Tamm, C.; Peik, E. Single-ion atomic clock with 3×10^{-18} systematic uncertainty. *Phys. Rev. Lett.* **2016**, *116*, 063001. [[CrossRef](#)] [[PubMed](#)]
9. Chou, C.W.; Hume, D.B.; Koelemeij, J.C.; Wineland, D.J.; Rosenband, T. Frequency comparison of two high-accuracy Al⁺ optical clocks. *Phys. Rev. Lett.* **2010**, *104*, 070802. [[CrossRef](#)] [[PubMed](#)]
10. Derevianko, A.; Pospelov, M. Hunting for topological dark matter with atomic clocks. *Nat. Phys.* **2014**, *10*, 933–936. [[CrossRef](#)]
11. Kolkowitz, S.; Pikovski, I.; Langellier, N.; Lukin, M.D.; Walsworth, R.L.; Ye, J. Gravitational wave detection with optical lattice atomic clocks. *Phys. Rev. D* **2016**, *94*, 124043. [[CrossRef](#)]
12. Blatt, S.; Ludlow, A.D.; Campbell, G.K.; Thomsen, J.W.; Zelevinsky, T.; Boyd, M.M.; Ye, J.; Baillard, X.; Fouche, M.; Le Targat, R.; et al. New limits on coupling of fundamental constants to gravity using ⁸⁷Sr optical lattice clocks. *Phys. Rev. Lett.* **2008**, *100*, 140801. [[CrossRef](#)] [[PubMed](#)]
13. Godun, R.M.; Nisbet-Jones, P.B.; Jones, J.M.; King, S.A.; Johnson, L.A.; Margolis, H.S.; Szymaniec, K.; Lea, S.N.; Bongs, K.; Gill, P. Frequency ratio of two optical clock transitions in ¹⁷¹Yb⁺ and constraints on the time variation of fundamental constants. *Phys. Rev. Lett.* **2014**, *113*, 210801. [[CrossRef](#)] [[PubMed](#)]
14. Huntemann, N.; Lipphardt, B.; Tamm, C.; Gerginov, V.; Weyers, S.; Peik, E. Improved limit on a temporal variation of m_p/m_e from comparisons of Yb⁺ and Cs atomic clocks. *Phys. Rev. Lett.* **2014**, *113*, 210802. [[CrossRef](#)] [[PubMed](#)]
15. Takano, T.; Takamoto, M.; Ushijima, I.; Ohmae, N.; Akatsuka, T.; Yamaguchi, A.; Kuroishi, Y.; Munekane, H.; Miyahara, B.; Katori, H. Geopotential measurements with synchronously linked optical lattice clocks. *Nat. Photon.* **2016**, *10*, 662–666. [[CrossRef](#)]
16. Grotti, J.; Koller, S.; Vogt, S.; Häfner, S.; Sterr, U.; Lisdat, C.; Denker, H.; Voigt, C.; Timmen, L.; Rolland, A.; et al. Geodesy and metrology with a transportable optical clock. *Nat. Phys.* **2018**, *14*, 437–441. [[CrossRef](#)]
17. Lisdat, C.; Grosche, G.; Quintin, N.; Shi, C.; Raupach, S.M.; Grebing, C.; Nicolodi, D.; Stefani, F.; Al-Masoudi, A.; Dorschner, S.; et al. A clock network for geodesy and fundamental science. *Nat. Commun.* **2016**, *7*, 12443. [[CrossRef](#)] [[PubMed](#)]
18. Takamoto, M.; Hong, F.L.; Higashi, R.; Katori, H. An optical lattice clock. *Nature* **2005**, *435*, 321–324. [[CrossRef](#)] [[PubMed](#)]
19. Campbell, S.L.; Hutson, R.B.; Marti, G.E.; Goban, A.; Darkwah Oppong, N.; McNally, R.L.; Sonderhouse, L.; Robinson, J.M.; Zhang, W.; Bloom, B.J.; et al. A fermi-degenerate three-dimensional optical lattice clock. *Science* **2017**, *358*, 90–94. [[CrossRef](#)] [[PubMed](#)]
20. Blatt, S.; Thomsen, J.W.; Campbell, G.K.; Ludlow, A.D.; Swallows, M.D.; Martin, M.J.; Boyd, M.M.; Ye, J. Rabi spectroscopy and excitation inhomogeneity in a one-dimensional optical lattice clock. *Phys. Rev. A* **2009**, *80*, 052703. [[CrossRef](#)]
21. Falke, S.; Misera, M.; Sterr, U.; Lisdat, C. Delivering pulsed and phase stable light to atoms of an optical clock. *Appl. Phys. B* **2012**, *107*, 301–311. [[CrossRef](#)]
22. Ma, L.S.; Jungner, P.; Ye, J.; Hall, J.L. Delivering the same optical frequency at two places: Accurate cancellation of phase noise introduced by an optical fiber or other time-varying path. *Opt. Lett.* **1994**, *19*, 1777–1779. [[CrossRef](#)] [[PubMed](#)]
23. Ye, J.; Peng, J.L.; Jones, R.J.; Holman, K.W.; Hall, J.L.; Jones, D.J.; Diddams, S.A.; Kitching, J.; Bize, S.; Bergquist, J.C. Delivery of high-stability optical and microwave frequency standards over an optical fiber network. *J. Opt. Soc. Am. B* **2003**, *20*, 1459–1467. [[CrossRef](#)]
24. Falke, S.; Lemke, N.; Grebing, C.; Lipphardt, B.; Weyers, S.; Gerginov, V.; Huntemann, N.; Hagemann, C.; Al-Masoudi, A.; Häfner, S.; et al. A strontium lattice clock with 3×10^{-17} inaccuracy and its frequency. *N. J. Phys.* **2014**, *16*, 073023. [[CrossRef](#)]
25. Wang, Y.B.; Yin, M.J.; Ren, J.; Xu, Q.F.; Lu, B.Q.; Han, J.X.; Guo, Y.; Chang, H. Strontium optical lattice clock at the national time service center. *Chin. Phys. B* **2018**, *27*, 023701. [[CrossRef](#)]

26. Boyd, M.M.; Zelevinsky, T.; Ludlow, A.D.; Blatt, S.; Zanon-Willette, T.; Foreman, S.M.; Ye, J. Nuclear spin effects in optical lattice clocks. *Phys. Rev. A* **2007**, *76*, 022510. [[CrossRef](#)]
27. Lu, B.Q.; Wang, Y.B.; Guo, Y.; Xu, Q.F.; Yin, M.J.; Li, J.G.; Chang, H. Experimental determination of the Landé g-factors for $5s^2\ ^1s$ and $5s5p\ ^3p$ states of the ^{87}Sr atom. *Chin. Phys. Lett.* **2018**, *35*, 043203. [[CrossRef](#)]
28. Olschewski, L. Messung der magnetischen Kerndipolmomente an freien ^{43}Ca -, ^{87}Sr -, ^{135}Ba -, ^{137}Ba -, ^{171}Yb - und ^{173}Yb -Atomen mit optischem Pumpen. *Zeitschrift für Physik* **1972**, *249*, 205–227. [[CrossRef](#)]
29. Bongs, K.; Singh, Y.; Smith, L.; He, W.; Kock, O.; Świerad, D.; Hughes, J.; Schiller, S.; Alighanbari, S.; Origlia, S.; et al. Development of a strontium optical lattice clock for the SOC mission on the ISS. *Comptes R. Phys.* **2015**, *16*, 553–564. [[CrossRef](#)]
30. Origlia, S.; Pramod, M.S.; Schiller, S.; Singh, Y.; Bongs, K.; Schwarz, R.; Al-Masoudi, A.; Dörscher, S.; Herbers, S.; Häfner, S.; et al. A high-performance optical lattice clock based on bosonic atoms. *Atomic Phys.* **2018**, arxiv:1803.03157.
31. Koller, S.B.; Grotti, J.; Vogt, S.; Al-Masoudi, A.; Dörscher, S.; Häfner, S.; Sterr, U.; Lisdat, C. Transportable optical lattice clock with 7×10^{-17} uncertainty. *Phys. Rev. Lett.* **2017**, *118*, 073601. [[CrossRef](#)] [[PubMed](#)]
32. Poli, N.; Schioppa, M.; Vogt, S.; Falke, S.; Sterr, U.; Lisdat, C.; Tino, G.M. A transportable strontium optical lattice clock. *Appl. Phys. B* **2014**, *117*, 1107–1116. [[CrossRef](#)]
33. Cao, J.; Zhang, P.; Shang, J.; Cui, K.; Yuan, J.; Chao, S.; Wang, S.; Shu, H.; Huang, X. A compact, transportable single-ion optical clock with 7.8×10^{-17} systematic uncertainty. *Appl. Phys. B* **2017**, *123*, 112. [[CrossRef](#)]
34. Zhao, F.J.; Gao, F.; Han, J.X.; Zhou, C.H.; Meng, J.W.; Wang, Y.B.; Guo, Y.; Zhang, S.G.; Chang, H. Miniaturization of physics system in Sr optical clock. *Acta Phys. Sin.* **2018**, *67*, 050601. [[CrossRef](#)]



© 2018 by the authors. Licensee MDPI, Basel, Switzerland. This article is an open access article distributed under the terms and conditions of the Creative Commons Attribution (CC BY) license (<http://creativecommons.org/licenses/by/4.0/>).